Competition Reactions of H 2 O •+ Radical in Concentrated Cl − Aqueous Solutions: Picosecond Pulse Radiolysis Study

ARTICLE *in* THE JOURNAL OF PHYSICAL CHEMISTRY A · NOVEMBER 2012

Impact Factor: 2.69 · DOI: 10.1021/jp309381z · Source: PubMed

5 AUTHORS, INCLUDING:

Abdel Karim El Omar
Lebanese University
11 PUBLICATIONS **110** CITATIONS
SEE PROFILE

Uli Schmidhammer
Université Paris-Sud 11
54 PUBLICATIONS **516** CITATIONS
SEE PROFILE

Mehran Mostafavi
Université Paris-Sud 11
162 PUBLICATIONS **2,910** CITATIONS
SEE PROFILE

THE JOURNAL OF PHYSICAL CHEMISTRY A

Article

pubs.acs.org/JPCA

Competition Reactions of $H_2O^{\bullet+}$ Radical in Concentrated Cl^- Aqueous Solutions: Picosecond Pulse Radiolysis Study

Abdel Karim El Omar,[†] Uli Schmidhammer,[†] Bernard Rousseau,[†] Jay LaVerne,[‡] and Mehran Mostafavi*[,†]

[†]Laboratoire de Chimie Physique/ELYSE, UMR 8000 CNRS/Université Paris—Sud 11, Orsay, France

[‡]Radiation Laboratory and Department of Physics, University of Notre Dame, Notre Dame, Indiana 46556, United States

ABSTRACT: Picosecond pulse—probe radiolysis measurements of highly concentrated Cl^- aqueous solutions are used to probe the oxidation mechanism of the Cl^-. The transient absorption spectra are measured from 340 to 710 nm in the picosecond range for the ultrafast electron pulse radiolysis of halide solutions at different concentrations up to 8 M. The amount of $Cl_2^{\bullet-}$ formation within the electron pulse increases notably with increasing Cl^- concentration. Kinetic measurements reveal that the direct ionization of Cl^- cannot solely explain the significant amount of fast $Cl_2^{\bullet-}$ formation within the electron pulse. The results suggest that Cl^- reacts with the precursor of the $OH^\bullet$ radical, i.e., $H_2O^{\bullet+}$ radical, to form $Cl^\bullet$ atom within the electron pulse and the $Cl^\bullet$ atom reacts subsequently with Cl^- to form $Cl_2^{\bullet-}$ on very short time scales. The proton transfer reaction between $H_2O^{\bullet+}$ and the water molecule competes with the electron transfer reaction between Cl^- and $H_2O^{\bullet+}$. Molecular dynamics simulations show that number of water molecules in close proximity decreases with increasing concentration of the salt (NaCl), confirming that for highly concentrated solutions the proton transfer reaction between $H_2O^{\bullet+}$ and a water molecule becomes less efficient. Diffusion-kinetic simulations of spur reactions including the direct ionization of Cl^- and hole scavenging by Cl^- show that up to 30% of the $H_2O^{\bullet+}$ produced by the irradiation could be scavenged for solutions containing 5.5 M Cl^-. This process decreases the yield of $OH^\bullet$ radical in solution on the picosecond time scale. The experimental results for the same concentration of Cl^- at a given absorbed dose show that the radiation energy absorbed by counterions is transferred to Cl^- or water molecules and the effect of the countercation such as Li^+, K^+, Na^+, and Mg^{2+} on the oxidation yield of Cl^- is negligible.

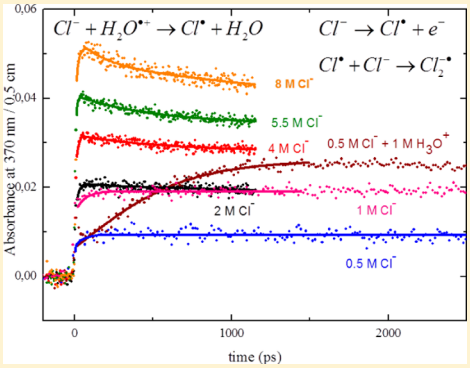

INTRODUCTION

Extensive studies on the radiolysis of water and aqueous solutions at low solute concentrations have been motivated by various applications in material and life sciences.[1,2] Product yields in dilute aqueous solutions can be predicted from the amount of water decomposition radicals at the end of the nonhomogenous stage, around 100 ns after energy deposition, and the rate coefficients for the reaction of those radicals with added solutes.[3,4] Hydrated electron yields have long been observed in the picosecond range, and new experimental developments have allowed the measurement of the radiolytic yield of the $OH^\bullet$ radical in the picosecond range.[5−7] Minor mechanisms in water radiolysis and very short time (subpicosecond) studies are still under investigation, but the radiolysis of pure water or aqueous solutions at low solute concentrations is now considered to be well-known up to the microsecond time scale. However, the situation is different when there is a possibility of direct interaction between solutes and radiation. This so-called direct effect occurs in the case of highly concentrated solutions where the solute is directly ionized (or oxidized or dissociated) by the radiation. The direct effect raises several fundamental questions in radiation chemistry, and it is also important for practical processes in nuclear energy technology as well as for radiotherapy.[1]

Examination of the direct effect was first performed in highly concentrated acidic solutions, which are used in the reprocessing of nuclear spent fuels.[8−14] Since salt mines are considered as repositories of radioactive waste, several studies have been conducted on the direct effect in halide solutions.[15−24] Quantification of the direct effect is also very important for biological systems. An estimated 50% of the DNA damage from γ-irradiation is due to the direct effects.[25] Recently, metal nanoparticle and cis-platinum complexes have been suggested to enhance the effect of radiation by using them as a secondary electron source.[26] For these reasons, an improved understanding of the radiation effects on solutes is crucial. In fact up to now, these types of effects in high solute concentrations are not quantitatively well established. Moreover, the fundamental water radiation chemistry could also be changed due to the interaction of water decomposition intermediates with solutes to produce new radicals at very short time scales. The investigation of such chemistry requires sophisticated time-resolved techniques. Picosecond pulse radiolysis is a powerful tool for the study of reactions in highly

Received: September 21, 2012
Revised: November 1, 2012
Published: November 1, 2012

   dx.doi.org/10.1021/jp309381z | J. Phys. Chem. A 2012, 116, 11509−11518

concentrated solutions. Thanks to a broad-band probe pulse and a multichannel detection system, the absorbance change of radical species in the UV and simultaneously that of the hydrated electron in the visible can be recorded under identical conditions in aqueous solution. Recent use of this method has shown that the radicals of solutes are formed through new mechanisms in highly concentrated nitric acid and halide solutions.[24] These mechanisms are insignificant in dilute solutions. In the case of halide solutions, preliminarily analysis of the pulse−probe measurements in the picosecond range suggested in highly concentrated halide solutions that $Br_2^{\bullet-}$ and $Cl_2^{\bullet-}$ can be formed within the electron pulse and before formation of their usual precursors $BrOH^{\bullet-}$ and $ClOH^{\bullet-}$, respectively.[24] This observation suggests that not only Br^- and Cl^- are directly oxidized by the electron pulse to form $Br^\bullet$ and $Cl^\bullet$ atoms, but that these anions can also undergo an oxidation reaction with the $H_2O^{\bullet+}$ radical. Such a process bypasses the reaction of halide anions with $OH^\bullet$ radicals. This process is surprising because in pure water the parent cation radical $H_2O^{\bullet+}$ is well-known to undergo a proton transfer reaction with another water molecule leading to the formation of the $OH^\bullet$ radical within a few tens of femtoseconds.[27,28] The reaction coordinate of this reaction is a vibration mode which is very fast, explaining why the proton transfer reaction is not directly observed using standard ultrafast techniques.

In the present work, we address the impact of high concentrations of Cl^- on the primary steps of radiation chemistry in water by combining extensive experimental studies with theoretical approaches. The exact local structure of the solutions before irradiation must be known in order to understand the mechanisms of radical reactions in highly concentrated solutions. This information has been obtained using molecular dynamics simulations to give the distance between the solute−water pairs and the change in the coordination number of the water molecule in highly concentrated NaCl aqueous solutions. New picosecond pulse radiolysis experiments have been performed with a series of highly concentrated Cl^- solutions to give detailed descriptions of the spur reactions in the picosecond range and to confirm our previous suggestion on the charge transfer from the precursor of $OH^\bullet$ radicals to the halide anions. A diffusion−kinetic model has been used to quantify the effect of the different oxidation reactions, including new mechanisms for the direct ionization of the solute and also for the fast electron transfer reaction of the solute with the $H_2O^{\bullet+}$ radical. The results show that the chemistry induced by the radiation in highly concentrated aqueous solutions is drastically different than in dilute solutions, and new pathways are required to explain the yield of oxidized Cl^- species observed in these solutions under irradiation.

EXPERIMENTAL SECTION

The purity of $MgCl_2$, NaCl, KCl, and LiCl was greater than 99.9%, and they were used as purchased from Sigma-Aldrich. Water was purified by passage through a Millipore purification system. The solutions were air saturated, and they were prepared at pH 6 as well as at pH 1. The pH of the solutions was adjusted with $HClO_4$. Salt solutions were investigated from 0.5 to 8 M Cl^-.

The picosecond pulse radiolysis experiments were performed at the experimental area EA-1 of the ELYSE facility. The electron accelerator based on radio-frequency photogun technology is described in detail elsewhere.[29,30] For the present experiments ELYSE was tuned to deliver electron pulses with energy of 7.1 MeV and a charge of around 4 nC at a repetition rate of the accelerator set to 10 Hz. ELYSE provides electron bunches in this configuration with a typical pulse duration around 10 ps and a rms shot-to-shot jitter less than 1 ps.[31,32]

The electron pump−optical probe setup is based on the laser-electron intrinsic synchronization resulting from the laser-triggered photocathode[33] and is detailed elsewhere.[15,34] Briefly, the main part of a femtosecond Ti:sapphire laser output is frequency tripled and used to produce the electron pulse that is accelerated by the RF fields. In the present work, about 1 μJ of the laser source was focused into a 6 mm thick CaF_2 disk to generate a supercontinuum covering the near UV and visible spectrum that was used as the optical probe. Probe and reference beam were each coupled into an optical fiber, transmitted to a spectrometer, and dispersed onto a CCD. The combination of the broad-band probe and the multichannel detector allows direct recording of the entire transient spectra independently of the shot-to-shot fluctuations and possible long-term drifts of the electron source. Crucial to the present work is the ability to record simultaneously the transient absorption of the radicals absorbing in the UV and that of the hydrated electron in the visible. The latter is used as the reference for the absorbed dose. The dose per pulse in pure water was determined by measuring the absorbance of the hydrated electron, $A_{e_{aq}^-}(\lambda, t)$, and by considering its initial yield measured at 10 ps to be $G(t = 20\ \text{ps}) = 4.2 \times 10^{-7}$ mol J^{-1}.[35] Therefore, the dose absorbed in water is given by

$$D_{\text{water}}(Gy) = \frac{A_{e_{hyd}^-}(\lambda, t)}{\varepsilon_\lambda l \rho_w G(t)} \quad (1)$$

where ε is the hydrated electron extinction coefficient (19 130 M^{-1} cm^{-1}, at maximum 718 nm),[36] l is the optical length, and ρ_w is the density of solution. All the measurements were made in a flow cell with a 5 mm optical path collinear to the electron pulse propagation. The absorbance measured for a given species in highly concentrated solutions is given by eq 2.

$$A(\lambda, t) = \varepsilon_\lambda l c(t) = \varepsilon_\lambda l F D_W G(t) \quad (2)$$

The dose additionally absorbed by the solute in concentrated solutions is obtained by multiplying the absorbed dose in pure water by the dose factor F

$$F = \rho_{\text{sol}}(Z_{\text{NaCl}} p/A_{\text{NaCl}} + Z_{\text{water}}(100 - p)/A_{\text{water}})\ (Z_{\text{water}} 100/A_{\text{water}})^{-1} \quad (3)$$

where ρ_{sol} is the density of the solution, Z is the number of electrons, A is the mass number, and p is the weight fraction of the solute per 100 g of solution. Solutions containing halide anions at high concentration and pure water were studied under identical experimental conditions. Particular attention was given to the use of a constant dose per pulse. Measurements were performed at 22.5 °C, the room temperature during the pulse radiolysis experiments.

Diffusion−Kinetic Methodology. The chemistry of an isolated spur was examined using a nonhomogeneous deterministic model in which the coupled differential equations for the various reactions were stepped in time using FACSIMILE, which is based on the Gear algorithm.[37] Water reactions, rate coefficients, and diffusion coefficients are the same as used previously.[38] The initial Gaussian spatial distributions were normalized using neat water radiolysis to

dx.doi.org/10.1021/jp309381z | J. Phys. Chem. A 2012, 116, 11509−11518

give reasonable agreement with the reported yields of 4.8 × 10^{-7} mol J^{-1} for the $OH^{\bullet}$ radical at 20 ps and 4.2 × 10^{-7} mol J^{-1} for the hydrated electron at 20 ps and by matching the observed decay of these two species in pure water up to 1 μs.[7,35] Best agreement to the observed data was obtained with initial (1 ps) yields of e_{aq}^-, $H_3O^{\bullet+}$, $H^{\bullet}$, H_2, and $OH^{\bullet}$, set to 4.4, 4.4, 0.3, 0.16, and 5.0 × 10^{-7} mol J^{-1}, respectively. The initial radius for e_{aq}^- was 2.8 nm, and a radius of 0.8 nm was used for all other species. Modeling the oxidation of Cl^- was performed by including the reaction scheme listed in Table 1. Rate coefficients for each of the Cl^- oxidation reactions were as given in the literature except for reactions 15 and 17, which were estimated from similar reactions with other halides.[39−46] The diffusion coefficients used were 2.1, 1.2, 1.1, 1.1, and 1.1 × 10^{-5} cm^2/s for $Cl^{\bullet}$, $Cl_2^{\bullet-}$, Cl_3^-, $ClOH^{\bullet-}$, and Cl_2, respectively.

Table 1. Reaction Scheme Used for the Oxidation of Cl^-

	reaction	k (M^{-1} s^{-1}) or (s^{-1})
R1	$OH^{\bullet} + Cl^- \rightarrow ClOH^{\bullet-}$	4.3 × 10^{939}
R2	$ClOH^{\bullet-} \rightarrow OH^{\bullet} + Cl^-$	6.1 × 10^{939}
R3	$Cl^{\bullet} + Cl^- \rightarrow Cl_2^{\bullet-}$	8.5 × 10^{943}
R4	$H^+ + ClOH^{\bullet-} \rightarrow Cl^{\bullet} + (H_2O)$	2.1 × 10^{1040}
R5	$ClOH^{\bullet-} \rightarrow Cl^{\bullet} + OH^-$	2.3 × 10^{140}
R6	$Cl^{\bullet} + OH^- \rightarrow ClOH^{\bullet-}$	1.8 × 10^{1040}
R7	$Cl_2^{\bullet-} \rightarrow Cl^{\bullet} + Cl^-$	6.0 × 10^{443}
R8	$Cl_2^{\bullet-} + Cl_2^{\bullet-} \rightarrow Cl_3^- + Cl^-$	2.0 × 10^{941}
R9	$Cl^{\bullet} + Cl_2^{\bullet-} \rightarrow Cl_3^-$	6.3 × 10^{842}
R10	$Cl^- + Cl_2 \rightarrow Cl_3^-$	1.0 × 10^{444}
R11	$Cl_3^- \rightarrow Cl^- + Cl_2$	5.0 × 10^{444}
R12	$Cl^{\bullet} + Cl^{\bullet} \rightarrow Cl_2$	8.8 × 10^{742}
R13	$e_{aq}^- + Cl^{\bullet} \rightarrow Cl^-$	1.0 × 10^{1045}
R14	$e_{aq}^- + Cl_2^{\bullet-} \rightarrow 2Cl^-$	1.0 × 10^{1045}
R15	$e_{aq}^- + Cl_3^- \rightarrow Cl^- + Cl_2^{\bullet-}$	3.0 × 10^{10}
R16	$H^{\bullet} + Cl^{\bullet} \rightarrow H^+ + Cl^-$	1.0 × 10^{1045}
R17	$H^{\bullet} + Cl_2^{\bullet-} \rightarrow H^+ + 2Cl^-$	8.0 × 10^{945}
R18	$H^{\bullet} + Cl_3^- \rightarrow H^+ + Cl^- + Cl_2^{\bullet-}$	1.0 × 10^{10}
R19	$HO_2^{\bullet} + Cl_2^{\bullet-} \rightarrow 2Cl^- + O_2 + H^+$	1.0 × 10^{946}

A nonhomogeneous deterministic model simplifies the physics by assuming an average spur, but it is fine for predicting the kinetics of fast electron radiolysis in the picosecond to microsecond regime. However, the approach is more uncertain on the subpicosecond time range associated with water decomposition and the reaction of fast transients such as $H_2O^{\bullet+}$. For this reason no attempt was made to model subpicosecond kinetics. The direct ionization of Cl^- to give $Cl^{\bullet}$ and e_{aq}^- was assumed to be proportional to the electron fraction of this component in the solution. The radiation chemical yield for this process was assumed to be the same as for the ionization of water, 4.4 × 10^{-7} mol J^{-1}. Electron fractions were obtained from the following equation

$$f_{NaCl}(M) = M_{NaCl} \times 28/(M_{NaCl} \times 28 + M_{H2O} \times 10) \quad (4)$$

where M_{NaCl} and M_{H_2O} are the measured molarities of NaCl and H_2O, respectively. Values of the molarities for the solutions studied here are given in Table 2. Scavenging of the $H_2O^{\bullet+}$ by Cl^- to give $Cl^{\bullet}$ was also not directly modeled but rather assumed to occur at some predetermined amount chosen to best match the experimental results. The yield of $Cl^{\bullet}$ formed by direct ionization of Cl^- or by scavenging of $H_2O^{\bullet+}$ was included in the initial (1 ps) yields and the amount of initial $OH^{\bullet}$ radical adjusted appropriately.

Molecular Dynamics Simulations. Molecular dynamics (MD) simulations of NaCl aqueous solutions were performed to study the effects of added solutes at high concentrations on the local water structure. Water was modeled using the flexible variant of the SPC/E model,[47] the SPC/Fw model.[48] This latter model was parametrized to better reflect dynamical and dielectric properties of bulk water, and it has been shown to reproduce many thermodynamical, dynamical, and structural properties better than most commonly used water models, except the rigid SPC/E model which is of comparable quality.[48] For sodium and chloride ions, the force field proposed by Wheeler and Newman was used.[49] This force field has been optimized to reproduce experimental solution densities and cation transference numbers when used in conjunction with the SPC/E model.

The simulations used our local code Newton.[50] Equations of motion were integrated using the velocity Verlet algorithm with a time step of 0.5 fs. A cutoff radius value of 1.2 nm was used for dispersion−repulsion interaction, and long-range corrections were added to potential energy and pressure.[51] The Ewald summation method was used to compute electrostatic interactions. Systems containing 12, 49, 103, and 145 NaCl molecules with 1321, 1297, 1297, and 1302 water molecules, respectively, were prepared in order to obtain four samples at 0.5, 2.0, 4.0, and 5.5 M. Samples were first equilibrated in the canonical ensemble and then in the isothermal−isobaric ensemble, using the explicit reversible ensemble for extended dynamics systems,[52] at 1 bar and 22.5 °C. The average density at all studied concentrations was computed from the NPT runs and used for production runs. Finally, trajectories were accumulated in the canonical ensemble for 1 ns and used to

Table 2. Chemical Composition of Aqueous Solutions Studied by Picosecond Pulse Radiolysis and the Corresponding Total Density, Dose Factor F, Electron Density Fraction of Solute f_s, and Electron Density Fraction of Water f_w

sample	composition	Cl^- (mol L^{-1})	water (mol L^{-1})	density (kg m^{-3})	F	f_s	f_w
1	pure water	0	55.56	1	1	0	1
2	NaCl	0.5	55	1.02	1.016	0.025	0.975
3	NaCl	1	54.1	1.03	1.03	0.05	0.95
4	NaCl	2	52.95	1.07	1.054	0.096	0.904
5	NaCl	4	50.34	1.15	1.108	0.182	0.818
6	NaCl	5.5	49.36	1.20	1.165	0.24	0.76
8	NaCl and 1 M $HClO_4$	1.0	54.1	1.016	1.03	0.05	0.95
9	LiCl	5.5	42.6	1.105	1.07	0.205	0.795
10	KCl	4	48.43	1.17	1.13	0.23	0.77
11	$MgCl_2$	8	24.82	1.26	1.156	0.426	0.574

dx.doi.org/10.1021/jp309381z | J. Phys. Chem. A 2012, 116, 11509−11518

Table 3. Calculated Density, Average Numbers of Water Molecules or Ions around a Water Molecule, N_w^x, and r_{min} Value Used in the MD Computation According to Eq 5

				water		Na^+		Cl^-	
[NaCl] (mol L^{-1})	experimental density, d_{exp} [64] (kg L^{-1})	calculated density, d_{cal} (kg L^{-1})	$(d_{cal} - d_{exp})/d_{exp}$ (%)	r_{min} (Å)	N_W^W	r_{min} r_{min} (Å)	N_W^{Na}	r_{min} (Å)	N_W^{Cl}
0.0	0.998	1.012 ± 0.001	1.4	3.31	4.41	–	–	–	–
0.5	1.019	1.030 ± 0.001	1.1	3.27	4.24	3.18	0.05	3.82	0.06
2.0	1.078	1.083 ± 0.001	0.5	3.23	3.86	3.18	0.21	3.82	0.26
4.0	1.152	1.147 ± 0.0025	- 0.4	3.15	3.19	3.18	0.41	3.82	0.55
5.5	1.200	1.185 ± 0.0025	−1.25	3.11	2.76	3.18	0.55	3.82	0.76

compute radial distribution functions $g(r)$. Coordination numbers between species i and j were derived from the radial distribution function of the corresponding species $g_{ij}(r)$, as the average number of molecules j inside a sphere of radius r_{min} from an arbitrary molecule i at the origin, n_i^j (r_{min})

$$n_i^j(r_{min}) = 4\pi\rho_j \int_0^{r_{min}} g_{ij}(r) r^2 dr \quad (5)$$

where ρ_j is the number density of particles j in the system and r_{min} corresponds to the first minimum in the radial distribution function.

RESULTS

The 10 different types of aqueous chloride solutions studied in this work by picosecond electron pulse radiolysis are listed in Table 2. For each solution, the dose factor F (see Experimental Section), the electron density fraction of water and solute, and the concentration of the water molecule are reported. Molecular dynamics simulations were performed on some of these systems to understand exactly the preirradiation configuration of the various components in these highly concentrated salt solutions. There is already a considerable amount of molecular dynamics studies on such systems: Several studies have focused on infinite dilution systems to study ion−water solvation shells and calculations of potential of mean force.[53−56] A large amount of simulation work has also been done at various concentrations to study ion pair association and evaluate contact ion pairs (CIP configurations) and solvent-separated ion pairs (SSIP configurations).[57−59] More recently, different experimental and simulation studies have focused on the local structure of water,[60−63] which is the most relevant quantity to understand competition reactions of fast transients of radiolytic products. Our molecular dynamics study is mostly dedicated to the determination of the structure of the first solvation shell of water molecules in a concentration range corresponding to the pulse radiolysis experiments.

Density values computed for the different water−NaCl mixtures at 22.5 °C and 1 bar are reported in Table 3. When compared with experimental data from Rogers and Pitzer,[64] there is a noticeable slight overestimation of densities at low salt concentration and underestimation of values at high concentration. However, discrepancies with experimental densities are small with the largest deviation being 1.25%. The behavior at low salt concentration is mostly due to the quality of the SPC/Fw model used here, which is known to slightly overestimate water density at ambient condition. The behavior at larger salt concentration reflects an underestimation of water−salt interactions, possibly because of the lack of a polarization effect. Moreover, the ion−water radial distribution functions (RDFs) and CIP and SSIP values are in agreement with literature values.[58] Therefore, the model can be considered to properly describe the local water environment in NaCl solutions.

RDFs for water−water pairs as computed from molecular dynamics are presented in Figure 1 with pure water rdf added

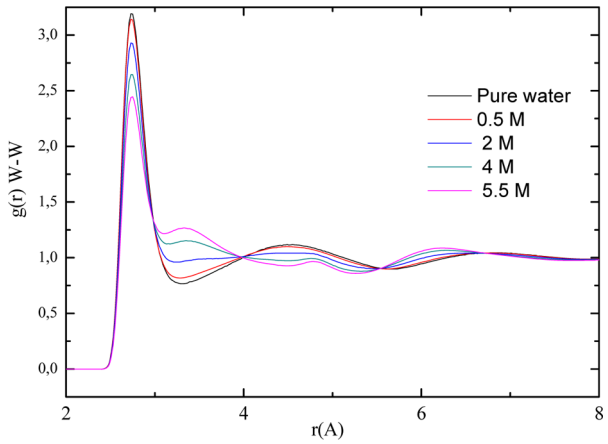

Figure 1. Water−water radial distribution functions for different NaCl concentration. $g(r)$ for pure water has been added for comparison.

for comparison. The water local structure is clearly modified by salt addition, in agreement with previous studies.[60,63,65] The intensity of the first peak (around 2.8 Å), which corresponds to H-bonded molecules, decreases with increasing salt concentration. The coordination number of water molecules (see Table 3), computed between $r = 0$ and the first local minimum at $r = r_{min}$ of the water−water rdf, decreases from 4.41 in pure water to 2.76 at 5.5 M concentration, showing that the probability of finding two water molecules in close proximity decreases with increasing salt concentration. As shown in Table 3, the water molecules leaving the first coordination shell of a water molecule are progressively replaced by sodium and chloride ions with increasing salt concentration. At larger distances, the rdf strongly evolves with salt concentration. This behavior was mentioned by Soper et al.,[63] who used molecular dynamics and an empirical potential structure refinement to obtain rdf based on neutron diffraction: the second peak of the water−water rdf mostly shifts toward the first peak with increasing salt concentration. Observation of this shift provides a strong validation of our simulations. Finally, the local structure is perturbed on a range extending up to 7 Å. This perturbation will affect the probability of proton transfer between the radiation produced $H_2O^{\bullet+}$ and the water molecule.

The radiolysis of Cl^- solutions reveals the typical signature of the hydrated electron with its large absorption band peaking in the red around 700 nm and an additional transient spectral band in the near UV that is attributed to the absorption of $ClOH^{\bullet-}$ and $Cl_2^{\bullet-}$ radicals. Figure 2 shows the normalized

dx.doi.org/10.1021/jp309381z | J. Phys. Chem. A 2012, 116, 11509−11518

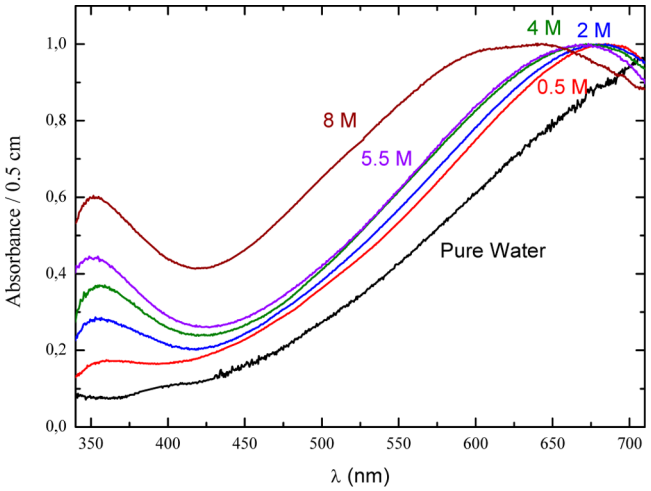

Figure 2. Normalized transient absorption spectra recorded directly after the picosecond electron pulse.

transient absorption spectra obtained immediately after the picosecond electron pulse. With increasing Cl^- concentration the overall absorption amplitude in the near UV increases, and a shift of the absorption band of the hydrated electron is induced to shorter wavelengths. In fact, the maximum of the absorption spectra of the hydrated electron around 700 nm is shifted to the blue by 10, 19, 23, 24, and 50 nm for 0.5, 2, 4, and 5.5 M NaCl and for 4 M $MgCl_2$ respectively. The shift for $MgCl_2$ is greater than that for NaCl because of the double charge and the small size of the cation. The position and shape of the absorption spectra of the hydrated electron are in agreement with previous spectra obtained for Na^+ solutions.[66,67] Such a spectral shift of the absorption band of the hydrated electron in highly concentrated salt solutions has been reported by several authors and is assigned to the electrostatic effect of the salt cations.[68]

The kinetics observed at 600 nm for an absorbed dose of 22.5 Gy in pure water is shown in Figure 3. The hydrated electron decay at this wavelength is attributed to its reactivity in spurs. Recently, we showed clearly that the transient absorption induced in the fused silica cell is not negligible and should be considered in picosecond pulse radiolysis of solutions in order to avoid errors on the time dependent yield of transient species.[69] This is why the contribution of the transient absorption in the fused silica cell (Figure 3, top inset) is already subtracted from the signals. The shape of the decay does not depend on the Cl^- concentration, except for the acidic solution. In acidic solutions, the hydrated electron decays very fast by reacting with H^+ with a corresponding value of the rate coefficient of 1.3×10^{10} M^{-1} s^{-1}. The spectra of Figure 2 clearly show that the amplitude of the absorbance at 600 nm increases with increasing Cl^- concentration. This increase is due two reasons: first the absorbed dose is not the same and should be corrected by the dose factor F and second the absorption spectra of the hydrated electron are blue-shifted and the extinction coefficients are not the same at 600 nm for different solutions. Normalization of the signals by the dose F factor (dose normalization) and including the changes in the extinction coefficients leads to a common kinetic curve as shown in Figure 3 (bottom), which suggests that the yield of the hydrated electron is almost the same in all of the solutions. Cerenkov light is observed to be more intense in the highly concentrated halides solutions due to the change of the

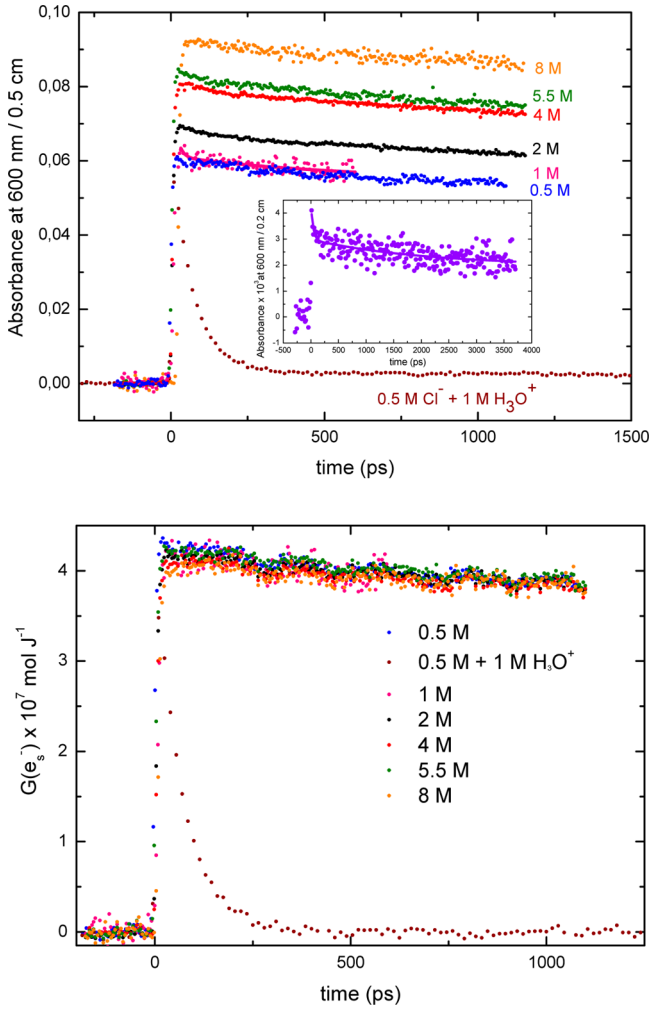

Figure 3. (Top) Decay recorded at 600 nm in aqueous solution and in pure water without any normalization. Inset: transient absorption induced in the windows of the empty optical fused silica cell. (Bottom) Time dependent yield of the hydrated electron decay recorded in aqueous solution. The yield is obtained by taking into account the shift of the absorption band (change of the extinction coefficient) and by dividing the decays by the dose (F factor).

refraction index. But, as the amount of hydrated electrons produced at a given absorbed dose is the same for the different studied solutions, here the contribution of the Cerenkov light to the fast formation of the atom halide is neglected. Hydrated electrons can be assumed to be produced by two mechanisms: direct water radiolysis and electron detachment of Cl^-:

$$H_2O \rightarrow H_2O^{+\bullet} + e^- \quad (6)$$

$$Cl^- \rightarrow Cl^\bullet + e^- \quad (7)$$

$$e^- \rightarrow \rightarrow e_s^- \quad (8)$$

Since the intensity of the probe light is lower at shorter wavelengths, the absorption of the oxidized species was observed at 370 nm, which is in the long-wavelength wing of their absorption bands. Figure 4(top) shows the observed kinetics at 370 nm where $ClOH^{\bullet-}$ and $Cl2^{\bullet-}$ radicals, the hydrated electron, and to a lesser extent the transient induced in the fused silica cell absorb. Figure 4(bottom) shows the absorbance due only to the oxidized species of Cl^- in solution following dose normalization (using the dose factor F), the

dx.doi.org/10.1021/jp309381z | J. Phys. Chem. A 2012, 116, 11509−11518

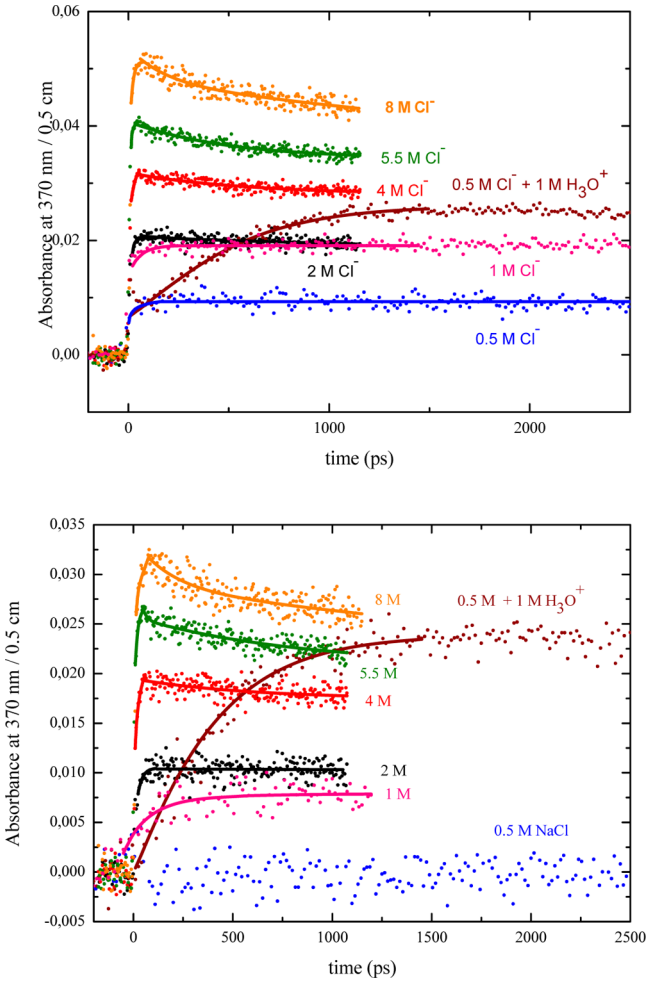

Figure 4. (Top) Transient absorption observed at 370 nm of aqueous solutions recorded from −300 ps to 1.5 ns at 370 nm. (Bottom) Contribution of the hydrated electron absorption and the transient signal of the irradiated fused silica cell at 370 are subtracted from the raw data presented in Figure 3 (top) to obtain transient absorption of the product of oxidation of Cl^- in aqueous solution. The solid lines are drawn to guide the eye.

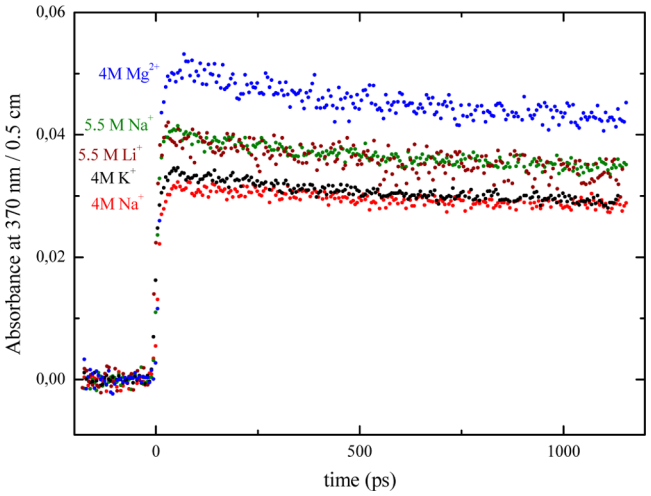

Figure 5. Transient absorption of the product of oxidation of Cl^- observed at 370 nm in aqueous solution of 4, 5.5, and 8 M Cl^- with different cations.

subtraction of hydrated electron absorption (which depends on the cation concentration), and subtraction of the transient induced in the fused silica cell (which cannot be avoided). For neutral solutions, the kinetics observed for the various concentrations of Cl^- ions are different. The initial amplitude of the signal for 0.5 M is very low and almost within the noise. The amplitude of the spectrum at 8 M Cl^- is the highest absorption after the pulse, and it is 1.27, 1.68, 3.2, and 3.9 times higher than that of 5.5, 4, 2, and 1 M Cl^- solutions, respectively. Moreover, the rise time for reaching the maximum is reduced from 1 to 8 M solutions. For 8 M Cl^- solutions the increase of the absorbance is very fast and in the range of the experimental time resolution (~20 ps), but in the case of 2 and 1 M solutions, the maximum of the absorbance is reached at around 150 and 500 ps, respectively. For the solution containing 0.5 M Cl^- and 1 M H^+, the absorbance reaches its maximum around 1.5 ns after the electron pulse and does not change until about 3.5 ns.

Kinetics traces at 370 nm are shown in Figure 5 at the same absorbed dose in solutions containing various types of chloride salts. Both the time decay and the amplitude are the same within the measurement sensitivity for solutions containing 4 and 5.5 M Cl^- and the counterions K^+ or Na^+ and Li^+ or Na^+, respectively. For the solution containing 4 M $MgCl_2$, the amplitude is higher because it contains 8 M Cl^-. These observations show that the counterion, even if it absorbs a part of the irradiation dose, does not change the kinetics of oxidized species of Cl^-. The solutions behave as if the energy deposited by the radiation is absorbed totally by water or directly by Cl^- through reactions 6 and 7, respectively. Energy may be absorbed by the cation, but the resulting cation (Na^{2+}, K^{2+}, Li^{2+}, or Mg^{3+}) instantaneously transfers the charge to Cl^- or to a water molecule. In highly concentrated solutions, pair formation is not negligible and the absorption of the dose by the NaCl is also transferred to Cl^-.

$$NaCl \xrightarrow{\text{irradiation}} (NaCl)^+ + e^- \rightarrow Na^+ + Cl^\bullet + e^- \qquad (9)$$

Therefore, the oxidized species such as Na^{2+}, Li^{2+}, K^{2+}, and Mg^{3+} are not stable in water, and they instantaneously oxidize water or Cl^- to form $H_2O^{\bullet+}$ and $Cl^\bullet$ by recovering their initial oxidation state Na^+, Li^+, K^+, and Mg^{2+}, respectively. The cation is just spectator and does not play a chemical role in these systems other than to induce a shift in the absorption band of the hydrated electron.

The predictions of the diffusion kinetic modeling of the spur for solutions containing 5.5 M Cl^- are shown in Figure 6 along with the observed transient absorption at 370 nm. Both $ClOH^{\bullet-}$ and $Cl_2^{\bullet-}$ radicals absorb at 370 nm with extinction coefficients of 3500 and 7300 M^{-1} cm^{-1}, respectively.[39] The model predictions for yields have been converted to absorbances using these extinction coefficients. Also shown in Figure 6 are the predicted yields for just the $Cl_2^{\bullet-}$ radical alone. The standard water radiolysis model gives too slow a buildup of products and predicts a maximum that is considerably lower than the observed absorbance. The direct ionization of Cl^- to give $Cl^\bullet$ and e_{aq}^- in 5.5 M Cl^- solutions can be included by assuming 0.24% of the energy is deposited directly into the Cl^-. This energy fraction is determined as described above and given in Table 2 for all the Cl^- concentrations in this work. Again the model predictions are too slow, and the maximum is lower than the observed absorbance. Clearly, the only method to increase the production of $ClOH^{\bullet-}$ and $Cl_2^{\bullet-}$ radicals on the

dx.doi.org/10.1021/jp309381z | J. Phys. Chem. A 2012, 116, 11509−11518

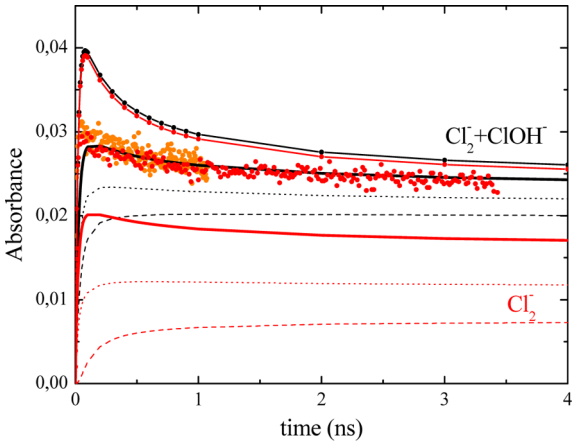

Figure 6. Observed absorbance decay (orange and red data for short and long time scale) with model simulations of spur reactions: (dashed line) simple water model alone without any direct effect; (dotted line) with direct ionization of Cl^-; (solid line) with direct ionization of Cl^- and 30% scavenging of $H_2O^{\bullet+}$ by Cl^-; and (dot–solid line) with direct ionization of Cl^- and 95% scavenging of $H_2O^{\bullet+}$ by Cl^- . The upper (black) curves are for the sum of $ClOH^{\bullet-}$ and $Cl_2^{\bullet-}$ radicals while the lower (red) curves are for $Cl_2^{\bullet-}$ radicals.

short time scale is to have a scavenging process for Cl^- reaction with a water transient species. Inclusion of the reaction of Cl^- with $H_2O^{\bullet+}$ increases the predicted absorbance with faster rise times. For 5.5 M Cl^- solution almost 30% of the $H_2O^{\bullet+}$ must be scavenged by Cl^- to match the observed absorbance measurements. In Figure 6 the solid black line presents this simulated absorbance which is in good agreement with the experimental data. That result is in agreement with the molecular dynamics simulations showing that the probability to find two water molecules in contact with each other decreases by increasing the concentration of NaCl.

DISCUSSION

After subtraction of the absorption of hydrated electron and transients from the fused silica cell, the two species $ClOH^{\bullet-}$ and $Cl_2^{\bullet-}$ are represented by the kinetics absorbing at 370 nm. At 370 nm the extinction coefficient of $ClOH^{\bullet-}$ (3500 M^{-1} cm^{-1}) is two times lower than that of $Cl_2^{\bullet-}$ (7300 $M^{-1}cm^{-1}$).[39] Moreover, the decomposition of $ClOH^{\bullet-}$ is fast ($k = 6.1 \times 10^9$ M^{-1} s^{-1}, reaction R2) compared to the $OH^\bullet$ radical scavenging reaction ($k = 4.3 \times 10^9$ M^{-1} s^{-1}, reaction R1) and the equilibrium reactions R1 and R2 are shifted toward the $OH^\bullet$ radical. The result of this equilibrium is that in neutral solution not all $OH^\bullet$ radicals are converted to $ClOH^{\bullet-}$.

$$OH^\bullet + Cl^- \rightarrow ClOH^{-\bullet} \quad \text{(R1)}$$

$$ClOH^{-\bullet} \rightarrow Cl^- + OH^\bullet \quad \text{(R2)}$$

Table 1 gives a complete set of the oxidation reactions of Cl^-. A simple estimate of the $OH^\bullet$ radical scavenging can be made by considering only the effect of Cl^- scavenging by reactions R1 and R2. This scavenging corresponds to the initial increase in the absorption shown in Figure 5. For the solutions containing 0.5, 2, 4, 5.5, and 8 M Cl^- concentration, the ratio of the expected yield of $ClOH^{\bullet-}$ on the initial $OH^\bullet$ radical yield is 0.23, 0.55, 0.71, 0.77, and 0.83, respectively. Considering the initial yield of $OH^\bullet$ radical within a few picoseconds of the electron pulse, even for 8 M Cl^- solutions the expected absorbance at the end of the pulse should be

$$\begin{aligned} A &= \varepsilon_{\lambda=370\text{nm}} lFDG_{ClOH^{-\bullet}} \\ &= 3500 \times 0.5 \times 22.5 \times 0.83 \times G_{OH^\bullet} \\ &= 0.016 \end{aligned} \quad (10)$$

which is two times lower than the observed value of 0.032 at 370 nm. For each solution, the values of the expected absorbance at the end of the pulse are reported in the Table 4. At Cl^- concentrations greater than 1 M, the observed

Table 4. Estimated $OH^\bullet$ Radical Scavenging[a]

$[Cl^-]$ (M)	$[ClOH^{-\bullet}]/[OH^\bullet]$	$G_{cal}(ClOH^{-\bullet})_{20\ ps}$ 10^7 mol J^{-1}	10^3 A_{cal} at 370 nm	10^3 A_{obs} at 370 nm	A_{obs}/A_{cac}
0.5	0.31	1.15	4.5	<4.5	<1
1	0.62	1.86	7.3	7.5	1.02
2	1.25	2.69	10.6	11.8	1.1
4	2.49	3.4	13.6	20	1.47
5.5	3.43	3.75	14.8	26.7	1.8
8	4.98	4.04	15.9	32.5	2.04

[a] G_{cal} and A_{cal} are the yield and absorbance calculated according to the scavenging by Cl^-. A_{obs} is the absorbance observed at 370 nm after data treatment (subtraction of hydrated electron and transients induced in fused silica cell).

absorbance is higher than the expected one. Obviously, the amount of $Cl_2^{\bullet-}$ formation within the pulse increases with increasing Cl^- concentration. This outcome can be rationalized by considering that $Cl_2^{\bullet-}$ can be formed within the electron pulse by two fast processes: first, the direct ionization of Cl^- in reaction 7 followed by the fast reaction of $Cl^\bullet$ to form $Cl_2^{\bullet-}$

$$Cl^\bullet + Cl^- \rightarrow Cl_2^{-\bullet} \quad \text{(R3)}$$

and, second, by oxidation of Cl^- with $H_2O^{\bullet+}$ followed by reaction R6.

$$Cl^- + H_2O^{\bullet+} \rightarrow Cl^\bullet + H_2O \quad (11)$$

In acidic solutions, the equilibrium reactions R1 and R2 are not important because of the fast proton reaction.

$$ClOH^{-\bullet} + H^+ \rightarrow Cl^\bullet + H_2O \quad \text{(R4)}$$

This difference between acid and neutral solutions is shown in Figure 4 for 0.5 M Cl^- solutions. Conversion of the $ClOH^{\bullet-}$ is relatively slow in acid solutions, but it continues to a much greater extent than in neutral solutions. One can readily see in Figure 4 that the total absorption in 0.5 M acid solutions very nearly matches that for 8 M Cl^- neutral solutions where the $OH^\bullet$ radical scavenging capacity is much higher due to the dominance of equilibrium reaction R1 over reaction R2.

Assuming an additively between direct and indirect effects of ionizing radiation, the radiolytic yield for a given transformation can be expressed by the following relation

$$G = f_s G_s + (1 - f_s) G_w \quad (12)$$

where f_s is the ratio of the energy directly absorbed by the solute S to the total energy absorbed by the solution and G_s is the radiolytic yield due to the direct effect. G_w is the yield of the indirect effect and expresses the yield of the radiolytic species formed in water that participate in the oxidization of Cl^-. Values of f_s are given in Table 2 for the various solutions used in this work. The value of G_s, the direct ionization of Cl^-, is assumed to be 4.4×10^{-7} mol J^{-1}, which is the same value as the ionization of water. However, model calculation results

dx.doi.org/10.1021/jp309381z | J. Phys. Chem. A 2012, 116, 11509–11518

shown in Figure 6 suggest that even the inclusion of the direct ionization of Cl^- is not sufficient to match the observed absorbance. The actual formation of the $ClOH^{\bullet-}$ and $Cl_2^{\bullet-}$ radicals occurs much faster and with a greater yield than the model predictions. Clearly, a very fast process must be responsible for formation of the $ClOH^{\bullet-}$ and $Cl_2^{\bullet-}$ radicals. Model calculations show that the dominant progression of events is the scavenging of $OH^\bullet$ radicals by Cl^-, reaction R1, followed by reactions R4 and R6 to give $Cl_2^{\bullet-}$ radical. The direct ionization of Cl^- gives the $Cl^\bullet$ radicals, which is again followed by reactions R3 to give $Cl_2^{\bullet-}$. Since very high concentrations of Cl^- are being used, the scavenging of water decomposition products is almost entirely possible. The most likely oxidizing species available for reaction with Cl^- is the $H_2O^{\bullet+}$. The reaction is obviously competing with neutralization and proton transfer reactions that are occurring on the femtosecond time scale.

The MD calculations show that the normal structure of water is different at high concentrations of Cl^-. With increasing Cl^- concentration there are on average less water molecules around each water molecule than in pure water. Proton transfer reactions from the $H_2O^{\bullet+}$ to water will be slightly less favored over reaction with Cl^-. The $Cl^\bullet$ radicals formed by the oxidation of Cl^- by the $H_2O^{\bullet+}$ will quickly undergo reactions R3 to give $Cl_2^{\bullet-}$ radicals. These reactions are essentially contact reactions and will occur instantly. Such reactions are far too fast to be included in the deterministic model used in this work. Their inclusion was accomplished by decreasing the initial yield of $OH^\bullet$ radicals with an equal addition of $Cl^\bullet$ radicals. The net result is a fractional decrease in the amount of decomposed water. Various values for this fraction were examined, and the results in Figure 6 show that a very good fit to the experimental data at 5.5 M Cl^- occurs when about 30% of the water decomposition is depleted. This fraction obviously depends on the initial Cl^- concentration, and no direct effects or variation in water decomposition are expected for solutions less than about 1 M Cl^-.

Scavenging the $H_2O^{\bullet+}$ by Cl^- is in essence converting the $OH^\bullet$ radicals to a different oxidizing species that then can participate in the evolution of the spur. The observed decay kinetics of the $OH^\bullet$ radical and the model predictions for this decay are shown in Figure 7. The time dependence of the $OH^\bullet$ radical decay is governed by the competition between its reactions with sibling radicals and diffusion out of the spur. The two main reactions of the $OH^\bullet$ radical are the one with the hydrated electron and combination reactions to produce H_2O_2. Formation of $Cl_2^{\bullet-}$ radical takes a few tens of picoseconds, but then the decay is very similar to that observed for the $OH^\bullet$ radical. However, the $Cl_2^{\bullet-}$ radical is the dominate species that is undergoing reaction on these time scales as can be observed for the model calculations for this species in Figure 6. In the same manner as the $OH^\bullet$ radical, the $Cl_2^{\bullet-}$ radical can react with the hydrated electron, reaction R14, or undergo combination reactions, reaction R8, to give Cl_3^-. Model calculations show a similar rate of production for both the H_2O_2 and the Cl_3^-. The kinetics of the $ClOH^{\bullet-}$ and $Cl_2^{\bullet-}$ radicals suggest that concentrated Cl^- solutions could be used in instances where one wants to convert $OH^\bullet$ radicals to different oxidizing species on very short time scales.

CONCLUSIONS

Picosecond pulse–probe radiolysis measurements of highly concentrated Cl^- aqueous solutions are used to probe the oxidation mechanism of the Cl^-. The concentration of the Cl^- was varied up to 8 M, and the transient absorption spectra were measured from 340 to 710 nm in the picosecond range. Of particular interest was the observation of the kinetics at 370 nm that corresponds after data treatment to the $ClOH^{\bullet-}$ and $Cl_2^{\bullet-}$ radicals. The amount of $ClOH^{\bullet-}$ and $Cl_2^{\bullet-}$ formation within the electron pulse increases notably with increasing Cl^- concentration. This increase is too large to be due to normal water radiolysis. Decomposition of Cl^- due to direct energy absorption is responsible for some of the observed product formation. Additional Cl^- oxidation must occur by its reaction with a very short-lived water decomposition transient. Diffusion–kinetic simulations of spur reactions including the direct ionization of Cl^- and hole scavenging by Cl^- show that up to 30% of the $H_2O^{\bullet+}$ produced by the irradiation could be scavenged for solutions containing 5.5 M Cl^-. The results suggest that Cl^- reacts with the precursor of the $OH^\bullet$ radical, i.e., $H_2O^{\bullet+}$ radical, to form $Cl^\bullet$ atom within the electron pulse, and the $Cl^\bullet$ atom reacts subsequently with Cl^- to form $Cl_2^{\bullet-}$ on the very short time scales. Proton transfer reaction between $H_2O^{\bullet+}$ and the water molecule competes with the electron

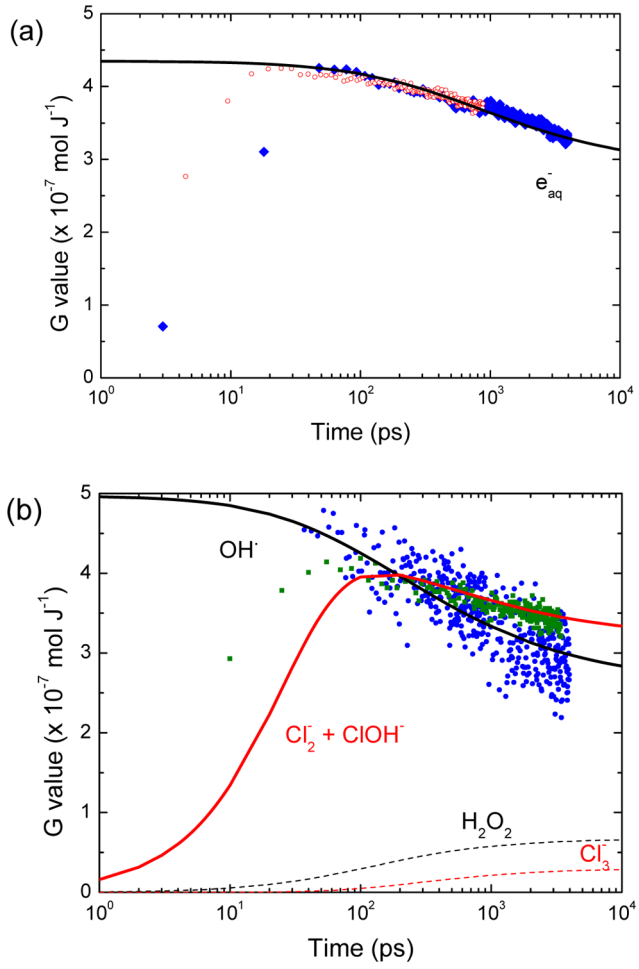

Figure 7. (a) Time dependence of the observed decay of the hydrated electron in pure water and the results of the model calculation. (b) Time dependence of the observed decay of $OH^\bullet$ radicals in pure water and the sum of $ClOH^{\bullet-}$ and $Cl_2^{\bullet-}$ radicals in 5.5 M Cl^- solutions. Model calculation results are shown for the decay of $OH^\bullet$ radicals and the formation of H_2O_2 in pure water and the formation and decay of $ClOH^{\bullet-}$ and $Cl_2^{\bullet-}$ radicals and the formation of Cl_3^- in 5.5 M Cl^- solutions.

dx.doi.org/10.1021/jp309381z | J. Phys. Chem. A 2012, 116, 11509–11518

transfer reaction between Cl^- and $H_2O^{\bullet+}$. This process decreases the yield of $OH^\bullet$ radical in solution on the picosecond time scale. Molecular dynamics simulations show that the number of hydrogen bonds between water molecules in the first shell decreases with increasing concentration of the salt, confirming that for highly concentrated solutions the proton transfer reaction between $H_2O^{\bullet+}$ and a water molecule becomes less efficient. The experimental results for the same concentration of Cl^- at a given absorbed dose show that the radiation energy absorbed by counterions is transferred to Cl^- or water molecules, and the effect of the countercation, such as Li^+, K^+, Na^+, and Mg^{2+}, on the oxidation yield of Cl^- is negligible.

AUTHOR INFORMATION

Corresponding Author

*E-mail: mehran.mostafavi@u-psud.fr.

Notes

The authors declare no competing financial interest.

ACKNOWLEDGMENTS

J.L. is thankful for the support of the University of Paris—Sud for a visiting position to develop the diffusion−kinetic model. His research described herein was also supported through the Division of Chemical Sciences, Geosciences and Biosciences, Basic Energy Sciences, Office of Science, United States Department of Energy through grant number DE-FC02-04ER15533. This is contribution number NDRL 4937 from the Notre Dame Radiation Laboratory.

REFERENCES

(1) Spotheim-Maurizot, M.; Mostafavi, M. Douki, T.; Belloni, J. *Radiation chemistry: From basics to applications in material and life science*; EDP Sciences: France, 2008.

(2) Hatano, Y.; Katsumura, Y.; Mozumder, A. *Charged particle and photon interactions with matter: Recent advances, applications and interfaces*; CRC Press: New York, 2011.

(3) Dewaele, V.; Lampre, I. Mostafavi, M. In *Charged particle and photon interactions with matter: Recent advances, applications and interfaces*; Hatano, Y., Katsumura, Y., Mouzumder, A., Eds.; CRC Press: New York, 2011; pp 289−324.

(4) Buxton, G. V. 2004. *The radiation chemistry of liquid water: Principles and applications*; Mozumder, A., Hatano, Y., Eds.; Marcel Dekker: New York, 2004; pp 331−363.

(5) Bartels, D. M.; Gosztola, D.; Jonah, C. D. *J. Phys. Chem. A* **2001**, *105*, 8069−8072.

(6) Muroya, Y.; Lin, M.; Wu, G.; Iijima, H.; Yoshi, K.; Ueda, T.; Kudo, H.; Katsumura, Y. *Radiat. Phys. Chem.* **2005**, *72*, 169−172.

(7) El Omar, A. K.; Schmidhammer, U.; Jeunesse, P.; Larbre, J.-P.; Lin, M.; Muroya, Y.; Katsumura, Y.; Pernot, P.; Mostafavi, M. *J. Phys. Chem. A* **2011**, *115*, 12212−12216.

(8) Matthews, R. W; Mahlman, H. A.; Sworski, T. J. *J. Phys. Chem.* **1972**, *76*, 2680−2684.

(9) Daniels, M. *J. Phys. Chem.* **1969**, *73*, 3710−3717.

(10) Kozlowska-Milner, E.; Broszkiewicz, R. K. *Radiat. Phys. Chem.* **1978**, *11*, 253−260.

(11) Pikaev, A. K.; Glazunov, P. Ya.; Yakubovich, A. *Akad. Dikl. Akad. Nauk SSSR* **1974**, *215*, 645−648.

(12) Lesigne, B.; Ferradini, C.; Pucheault, J. *J. Phys. Chem.* **1973**, *17*, 2156−2158.

(13) Katsumura, Y; Jiang, P. Y.; Nagaishi, R.; Oishi, T.; Ishigure, K.; Yoshida, Y. *J. Phys. Chem.* **1991**, *95*, 4435−4439.

(14) Balcerzyk, A.; El Omar, A. K.; Schmidhammer, U.; Pernot, P.; Mostafavi, M. *J. Phys. Chem. A* **2012**, *116*, 7302−7307.

(15) Pucheault, J.; Ferradini, C.; Julien, R.; Deysine, A.; Gilles, L.; Moreau, M. *J. Phys. Chem.* **1978**, *83*, 330−336.

(16) Hadjadj, A.; Julien, R.; Pucheault, J.; Ferradini, C.; Hickel, B. *J. Phys. Chem.* **1982**, *86*, 4630−4634.

(17) Woods, R. J.; Lesigne, B.; Gilles, L.; Ferradini, C.; Pucheault, J. *J. Phys. Chem.* **1975**, *79*, 2700−2704.

(18) Schuler, R. H.; Hartzell, A. L.; Behar, B. *J. Phys. Chem.* **1981**, *85*, 192−199.

(19) Atinault, E.; De Waele, V.; Schmidhammer, U.; Fattahi, M.; Mostafavi, M. *Chem. Phys. Lett.* **2008**, *460*, 461−465.

(20) Grigor'eva, A. E.; Makarov, I. E.; Pikaev, A. K. *High Energy Chem.* **1991**, *25*, 172−176.

(21) Mirdamadi-Esfahani, M.; Lampre, I.; Marignier, J. -L.; De Waele, V.; Mostafavi, M. *Radiat. Phys. Chem.* **2009**, *78*, 106−111.

(22) Balcerzyk, A.; LaVerne, J.; Mostafavi, M. *J. Phys. Chem. A* **2011**, *115*, 4326−4333.

(23) Katsumura, Y. *Radiation chemistry: Present status and future trends (Studies in physical and theoretical chemistry)*; Jonah, C. D., Rao, B. S. M., Eds.; Elsevier: New York, 2001; Vol. *87*, pp 163−174.

(24) Balcerzyk, A.; Schmidhammer, U.; El Omar, A. K.; Jeunesse, P.; Larbre, J.-P.; Mostafavi, M. *J. Phys. Chem. A* **2011**, *115*, 9151−9159.

(25) Bernhard, W. A.; Close, D. M. *DNA damage dictates the biological consequence of ionizing radiation: The chemical pathway, in charged particle and photon interactions with matter*; Hatano, Y., Mozumder, A., Eds.; Marcel Dekker: New York, 2004; pp 431−470.

(26) Brun, E.; Duchambon, P.; Blouquit, Y.; Keller, G.; Sanche, L.; Sicard-Roselli, C. *Radiat. Phys. Chem.* **2009**, *78*, 177−183.

(27) De Waele, V.; Lampre, I.; Mostafavi, M. *Charged particle and photon interactions with matter*; Hatano, Y., Katsumura, Y., Mozumder, A., Eds.; CRC Press: New York, 2011; pp 289−324.

(28) Garrett, B. C.; Dixon, D. A.; Camaioni, D. M.; Chipman, D. M.; Johnson, M. A.; Jonah, C. D.; Kimmel, G. A.; Miller, J. H.; Rescigno, T. N.; Rossky, P. J.; et al. *Chem. Rev.* **2005**, *105*, 355−390.

(29) Belloni, J.; Monard, H.; Gobert, F.; Larbre, J. -P.; Demarque, A.; De Waele, V.; Lampre, I.; Marignier, J. -L.; Mostafavi, M.; Bourdon, J. C.; et al. *Nucl. Instrum. Methods Phys. Res., Sect. A* **2005**, *539*, 527−539.

(30) Marignier, J. L.; De Waele, V.; Monard, H.; Gobert, F.; Larbre, J.-P.; Demarque, A.; Mostafavi, M.; Belloni, J. *Radiat. Phys. Chem.* **2006**, *75*, 1024−1033.

(31) Schmidhammer, U.; De Waele, V.; Marquès, J.-R.; Bourgeois, N.; Mostafavi, M. *Appl. Phys. B: Lasers Opt.* **2009**, *94*, 95−101.

(32) De Waele, V.; Schmidhammer, U.; Marquès, J.-R.; Monard, H.; Larbre, J.-P.; Bourgeois, N.; Mostafavi, M. *Radiat. Phys. Chem.* **2009**, *78*, 1099−1101.

(33) Belloni, J. ; Crowell, R. A.; Katsumura, Y.; Lin, M.; Marignier, J. -L.; Mostafavi, M.; Muroya, Y.; Akinori, S.; Tagawa, S.; Yoshida, Y. De Waele, V.; Wishart, J. F. In *Recent trends in radiation chemistry*; Wishart, J. F., Rao, B. S. M., Eds.; World Scientific: Hackensack, NJ, 2010; pp 121−160.

(34) Schmidhammer, U.; Pernot, P.; De Waele, V.; Jeunesse, P.; Demarque, A.; Murata, S.; Mostafavi, M. *J. Phys. Chem. A* **2010**, *114*, 12042−12051.

(35) Muroya, Y.; Lin, M.; Wu, G.; Iijima, H.; Yoshii, K.; Weda, T.; Kudo, H.; Katsumura, Y. *Radiat. Phys. Chem.* **2005**, *72*, 169−172.

(36) Jou, F. Y.; Freeman, G. R. *J. Phys. Chem.* **1977**, *81*, 909−915.

(37) Chance, E. M.; Curtis, A. R.; Jones, I. P.; Kirby, C. R. Report AERE-R 8775; AERE: Harwell, U.K., 1977.

(38) LaVerne, J. A.; Pimblott, S. M. *J. Phys. Chem.* **1991**, *95*, 3196−3206.

(39) Jayson, G. G.; Parsons, B. J.; Swallow, A. J. *J. Chem. Soc., Faraday Trans.* **1973**, *69*, 1597−1607.

(40) Klaning, U. K.; Wolff, T. *Ber. Bunsen-Ges. Phys. Chem.* **1985**, *89*, 243−245.

(41) Ferraudi, G. *J. Phys. Chem.* **1993**, *97*, 2793−2797.

(42) Wu, D.; Wong, D.; DiBartolo, B. *J. Photochem.* **1980**, *14*, 303−310.

(43) Buxton, G. V.; Bydder, M.; Salmon, G. A. *J. Chem. Soc., Faraday Trans.* **1998**, *94*, 653−657.

(44) Bjergbakke, E.; Draganic, Z. D.; Sehested, K.; Draganic, I. G. *Radiochim. Acta* **1989**, *48*, 73−77.
(45) Draganic, I. G.; Bjergbakke, E.; Draganic, Z. D.; Sehested, K. *Precambrian Res.* **1991**, *52*, 337−345.
(46) Navaratnam, S.; Parsons, B. J.; Swallow, A. J. *Radiat. Phys. Chem.* **1980**, *15*, 159−161.
(47) Berendsen, H. J. C.; Grigera, J. R.; Straatsma, T. P. *J. Phys. Chem.* **1987**, *91*, 6269−6271.
(48) Wu, Y.; Tepper, H. L.; Voth, G. A. *J. Chem. Phys.* **2006**, *124*, 024503.
(49) Wheeler, D. R.; Newman, J. *J. Phys. Chem. B.* **2004**, *108*, 18353−18361.
(50) Nguyen, T. V.-O.; Houriez, C.; Rousseau, B. *Phys. Chem. Chem. Phys.* **2010**, *12*, 930−6.
(51) Allen, M. P.; Tildesley, D. J. *Computer simulation of liquids*; Oxford Science Publications: Oxford, U.K., 1989.
(52) Martyna, G. J.; Tuckerman, M.; Tobias, D.; Klein, M. *Mol. Phys.* **1996**, *87*, 1117−1157.
(53) Zhu, S.-B.; Robinson, G. W. *J. Chem. Phys.* **1992**, *97*, 4336.
(54) Chialvo, A. A.; Cummings, P. T.; Cochran, H. D.; Simonson, J. M.; Mesmer, R. E. *J. Chem. Phys.* **1995**, *103*, 9379.
(55) Dang, L. *J. Am. Chem. Soc.* **1995**, *117*, 6954−6960.
(56) Lyubartsev, A. P.; Laaksonen, A. *Phys. Rev. E.* **1995**, *52*, 3730−3737.
(57) Hummer, G. *J. Phys.: Condens. Matter* **1994**, *6*, A141−A144.
(58) Lyubartsev, A. P.; Laaksonen, A. *J. Phys. Chem.* **1996**, *100*, 16410−16418.
(59) Degrève, L.; da Silva, F. L. B. *J. Chem. Phys.* **1999**, *110*, 3070.
(60) Chandra, A. *Phys. Rev. Lett.* **2000**, *85*, 768−71.
(61) Chowdhuri, S.; Chandra, A. *Phys. Rev. E* **2002**, *66*, 1−7.
(62) Beladjine, S.; Amrani, M.; Zanoun, A.; Belaidi, A.; Vergoten, G. *Comput. Theor. Chem.* **2011**, *977*, 97−102.
(63) Mancinelli, R.; Botti, A.; Bruni, F.; Ricci, M. A.; Soper, A. K. *Phys. Chem. Chem. Phys.* **2007**, *9*, 2959−67.
(64) Rogers, P. S. Z.; Pitzer, K. S. *J. Phys. Chem. Ref. Data.* **1982**, *11*, 15.
(65) Carrillo-Tripp, M.; Saint-Martin, H.; Ortega-Blake, I. *J. Chem. Phys.* **2003**, *118*, 7062.
(66) Wolff, R. K.; Aldrich, J. E.; Penner, T. L.; Hunt, J. W. *J. Phys. Chem.* **1975**, *79* (3), 210−219.
(67) Anbar, M.; Hart, E. J. *J. Phys. Chem.* **1965**, *69* (4), 1244−1247.
(68) Bonin, J.; Lampre, I.; Mostafavi, M. *Radiat. Phys. Chem.* **2005**, *74*, 288−296.
(69) Schmidhammer, U.; El Omar, A. K.; Balcerzyk, A.; Mostafavi, M. *Radiat. Phys. Chem.* **2012**, *81*, 1715−1719.